SEMMELWEIS EGYETEM

DOKTORI ISKOLA

Ph.D. értekezések

3302.

SZADAI ZOLTÁN

Funkcionális Idegtudományok

című program

Programvezető: Dr. Sperlágh Beáta, egyetemi tanár

Témavezető: Dr. Rózsa Balázs, csoportvezető

REPRESENTATION OF REINFORCEMENT SIGNALS IN THE NEOCORTEX BY VASOACTIVE INTESTINAL POLYPEPTIDE-EXPRESSING INTERNEURONS

PhD thesis

Zoltán Szadai, MD

János Szentágothai Neurosciences Division

Semmelweis University

Supervisor: Balázs Rózsa, MD, Ph.D

Official reviewers: János Réthelyi, MD, Ph.D
Richárd Fiáth Ph.D

Head of the Complex Examination Committee: Árpád Dobolyi, Ph.D

Members of the Complex Examination Committee: Róbert Bódizs, Ph.D
Nikolett Lénárt, Ph.D

Budapest
2025

Table of Contents

List of Abbreviations

ACx – auditory cortex

AO – acousto-optic

Ca^{2+} – calcium

CCK – cholechystokinin

CMOS – complementary metal-oxide semiconductor

CR – calretinin/correct rejection

DSI – direction selectivity index

FA – false alarm

FWHM – full witdth at half maximum

GABA – gamma-aminobutyric acid

GRP – gastrin-releasing peptide

Hz – Hertz

Kg – kilogram

kHz – kilohertz

L2/3 – layer 2/3

LCD – liquid-crystal display

M1 – primary motor cortex

mg – milligram

mPFC – medial prefrontal cortex

mPTA – medial parietal cortex

µm – micrometer

nl – nanoliter

OSI – orientation selectivity index

PCA – principal component analysis

PTA – parietal cortex

PV – parvalbumin

RL – reinforcement learning

s – second

S1 – primary somatosensory cortex

SD – standard deviation

SEM – standard error of the mean

SNR – signal-to-noise ration

SOM – somatostatin

SWR – sharp-wave ripple

tSNE – T-distributed stochastic neighbor embedding

V1 – primary visual cortex

VIP – vasoactive intestinal polypeptide

1. Introduction

1.1 Predictive coding in the brain

As early as the second half of the 19th century, a theory was posited that the brain possesses the capacity to predict future events. This theory is attributed to Hermann von Helmholtz, an eminent ophthalmologist and theoretical researcher (1). Helmholtz observed that when patients with unilateral trauma to the lateral rectus muscle close their healthy eye and attempt to look rightward with the affected right eye, they perceive a rapid shift of the external world in the rightward direction. In contrast, a healthy individual performing the same action does not experience such a phenomenon, despite the relative change in the position of the eye to the external world due to the eye's motion (2).

From this observation, Helmholtz inferred the necessity of a cerebral compensatory mechanism that corrects the displacement of images resulting from eye movements, thus maintaining visual stability (1).

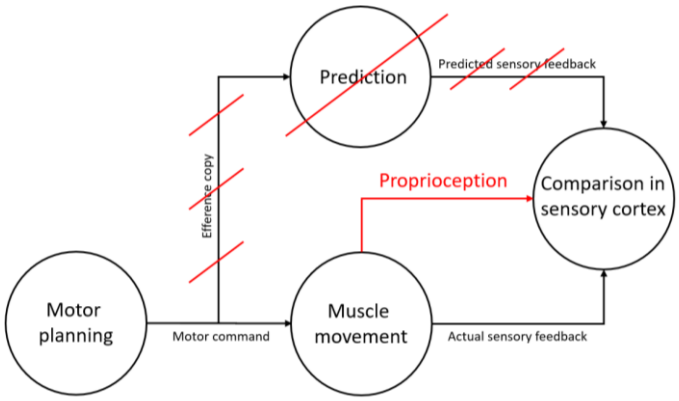

Figure 1. Comparison of proposed pathways of information from motor to sensory cortices in von Helmholz's and Sherington's (red) view (modified from (3)).

This was a theory that could not be proven under the circumstances at the time, as the neurophysiological tools necessary for such investigations were not available. However, it served as a good framework for theoretical thinking in explaining perception and its pathological deviations.

A prominent proponent of this perspective was Charles Sherrington, who discovered proprioceptors in muscles and believed it more economical to utilize information from these muscle fiber shortenings for necessary corrections in the sensory systems due to one's own movements (**Figure 1**) (4). Although this mechanism could not fully explain Helmholtz's observation, the predictive coding theory has been sidelined (1). For instance, in a medical physiology textbook written in the 2010s, there is only a single mention of predictive coding in the context of the spinal system regulating posture (5).

However, beneath the surface — especially among theoreticians — the concept of prediction error was implicitly embedded in their thinking. For example, it was also inherent in the Rescorla-Wagner model, which offers a simple yet effective mathematical framework for reinforcement learning (6).

Beginning in the 1990s, researchers started to document phenomena, that were not easily explainable within the framework of representational theories. These discoveries were related to the functioning of the dopaminergic system. Wolfram Schulz observed that the release of the neurotransmitter dopamine increased in specific brain regions (ventral tegmental area and substantia nigra) when an animal received a reward (7). However, if this reward was associated with a predictive cue, the dopaminergic neurons shifted their increased activity to respond to the cue rather than the reward itself (**Figure 2**). If the presentation of the predictive cue was not followed by a reward, the neurons decreased their firing rate (7).

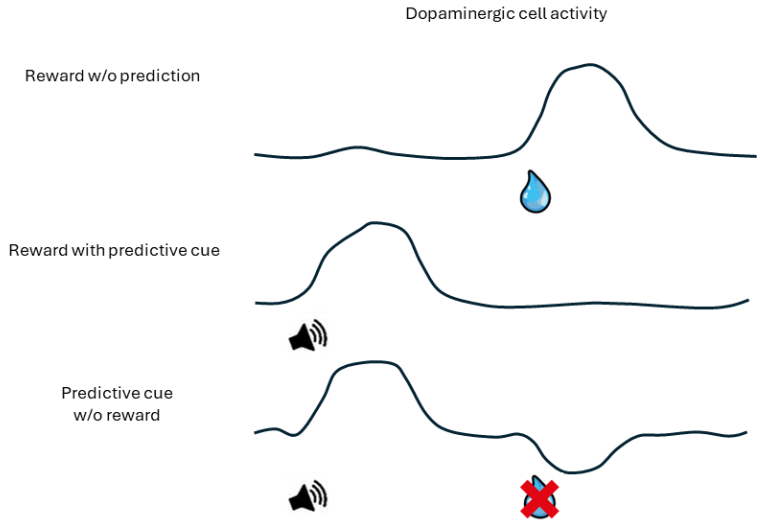

Figure 2. Dopaminergic cell activity tracks reward and predictive cue presentation (original figure).

Subsequently, researchers described a mechanism within the cerebral cortex that aligned with the predictive framework. In one particular experiment, mice ran in a virtual straight-line maze, where the virtual reality changed in sync with their movement. It was noted that when the connection between the mouse's movement and the virtual reality was temporarily disrupted - such that the maze appeared stationary despite the mouse's continued running -, a significant proportion of supragranular (L2/3) cells increased their activity in primary visual cortex (8, 9). This effect was less pronounced in deeper-lying cells (10). This experimental series modeled what happens when the coordinate systems of the motor and visual systems are decoupled. The heightened activity of L2/3 pyramidal cells could indicate the signaling of a prediction error. It's also hypothesized that the subgranular system may represent internal models of the external world, allowing for the comparison of information derived from both the motor and visual systems (1). Somatostatin (SOM) containing interneurons, responsible for inhibition caused by visual inputs, played a crucial role (8). Theoretically, during a mismatch, those principal neurons were activated which received excitatory inputs from the motor cortex, while simultaneously receiving inhibitory inputs from SOM interneurons. As the visual flow halted, these inhibitory inputs subsided, enabling cell activation by the motor inputs. It's important to mention that some argue this is not a signaling of prediction error; rather,

neurons that were more sensitive to stationary (still) bars compared to moving ones were mistakenly identified as signaling prediction error (11).

Although it is crucial for organisms to discern advantageous or detrimental events in each environment, our understanding of how this is realized at the level of neuronal circuits and how this information is conveyed to the cerebral cortex is limited. Notably, the dopaminergic system, responsible for reward processing, projects mainly to the anterior and the middle regions of the cortex (12). In contrast, other major neuromodulator systems send axons to the entire cerebral cortex (13-15). It has been demonstrated that information related to rewards appears in the cholinergic basal forebrain (16-18), in the noradrenergic central hub locus coeruleus (19, 20), and also in the serotonergic nuclei of the median raphe (21). Predictive coding-related modulation was also observed in both the cholinergic and noradrenergic systems (20, 22). These anatomical pathways could serve as good candidates to disperse information about reinforcement to the neocortex.

1.2 VIP interneurons in the canonical cortical microcircuits

Pyramidal cells are the predominant cell type in the neocortex, constituting approximately 75-80% of all cortical neurons (23). The remaining portion comprises the class of interneurons, of which around 85% can be categorized into distinct groups based on their content of parvalbumin, somatostatin, or vasoactive intestinal polypeptide (24). These interneurons primarily regulate the activity of pyramidal cells and each other through the neurotransmitter gamma-aminobutyric acid (GABA). The innervation patterns they follow are relatively consistent across the entire cerebral cortex (25-28), as well as in the hippocampus (29-32) and the amygdala region (33). This pattern is characterized as follows: PV (parvalbumin) -containing interneurons synapse with the soma of pyramidal cells, maintaining inhibitory control over them. SOM interneurons perform a similar function with the dendrites of pyramidal cells. VIP interneurons inhibit, to a lesser extent, PV interneurons and more significantly, SOM interneurons. Consequently, relative to pyramidal cells, VIP interneurons exert a disinhibitory effect (**Figure 3**). Additionally, they directly inhibit these cells to some extent. The inputs of VIP interneurons are coming from nearby neurons and also from distant areas like thalamus (34), and from

neuromodulators like serotonin (35) and acetylcholine (25, 36). Interestingly, gastrin-releasing peptide (GRP) can also activate these interneurons and drives the disinhibitory circuit in order to support fear memory formation (37).

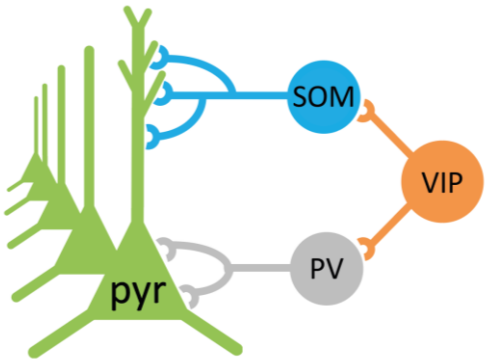

Figure 3. A canonical cortical disinhibitory circuit (original figure).

In terms of function, VIP interneurons play a role in sensory processing, with their significance varying across different modalities. For instance, in the V1, they were found to be broadly tuned, while in the auditory cortex, a sharp intensity tuning was observed (38). However, overall, their specificity is weaker compared to pyramidal cells (28, 39-42). Their role in mediating context has also been described: they remained quiet when the center and the surrounding of a visual stimulus was identically oriented but were activated when the two differed (43). A particularly specific trait of VIP interneurons is their population-level activation during the animal's locomotion or in high arousal states, a response not shared by other cell types: SOM interneurons tend to be inhibited, while pyramidal cells show heterogeneous responses (44).

Like PV and SOM interneurons, VIP interneurons also influence learning. Inhibiting the development or directly the activity of VIP interneurons in different cortical regions during learning tasks that utilize various modalities was shown to decrease behavioral performance (45-49). They were shown to be specifically connected to symptoms such as hypersensitivity to distractors in genotypes commonly associated with autism spectrum disorder (50).

An interesting debate is unfolding regarding the role of sensory prediction errors in modulating the activity of VIP interneurons. They were activated in a visual change detection task by novel images and suppressed after presenting familiar ones (51). In contrast, a study using a visual oddball paradigm demonstrated elevated activity in VIP interneurons in response to redundant, rather than deviant, stimuli (52). The divergent findings of these studies may be partly attributable to the use of different behavioral paradigms. The significance of this topic is derived from the role of deviance detection as an extensively described experimental model for mismatch negativity, recognized as an objective biomarker of schizophrenia (52).

2. Objectives

The starting point of my work was the observation that during an auditory discrimination task, VIP interneurons were activated not only in response to auditory stimuli but also following the reward (28). My research aimed to illuminate whether this type of recruitment could be applicable to the entire neocortex. Given the role of VIP interneurons within local microcircuits, this could potentially serve as a global teaching signal, facilitating the association between predictive cues and reinforcement. While VIP interneuron activity post-reinforcement has been observed in other regions alongside other cell types – in the hippocampus and medial prefrontal cortex (mPFC) following rewards, and in the amygdala in relation to punishment (33, 53, 54) – this aligns well with the functional roles of these specific brain regions. However, in the primary visual and somatosensory cortices, no post-reward increase in activity was observed (40, 42), raising questions about the existence of a global teaching signal. Therefore, I systematically measured the activity of VIP interneurons across several areas of the neocortex using a custom-developed three-dimensional acousto-optical 2-photon microscope while mice performed an auditory discrimination task.

3. Methods

3.1 Animals

The experimental animals used in this study included the following strains: VIP-Cre, PV-Cre, and Thy1-Cre mice (*Vip*$^{tm.1(cre)Zjh}$/J, B6.129P2-*Pvalb*$^{tm1(cre)Arbr}$/J, FVB/N-*Tg(Thy1-cre)1Vln*/J, from The Jackson Laboratory). Individuals of both sexes, aged between 6-24 weeks were selected. They were housed in small groups in a controlled environment with regulated temperature and humidity, and a reversed light-dark cycle. Upon commencement of behavioral training, their water intake was restricted to 1 ml/day, with unlimited access to food. All procedures adhered to the guidelines of the Animal Care and Experimentation Committee of the Institute of Experimental Medicine of the Hungarian Academy of Sciences, in accordance with Hungarian and EU regulations.

3.2 Surgical procedure

Following inhalation of isoflurane, the animals were anesthetized using a mixture of anesthetics (fentanyl, midazolam, and medetomidine at 0.05 mg, 5 mg, and 0.5 mg/kg, respectively) administered intraperitoneally. They were secured in a stereotaxic frame, placed on a heating pad, and ophthalmic ointment was applied to their eyes. A 0.2% Ropivacaine anesthetic was injected into the scalp to the surface of the skull. The scalp was then shaved and removed. After cleaning and drying the skull bone with 3% hydrogen peroxide, a craniotomy was created using a biopsy punch and a dental drill: the outline of the craniotomy was marked with a 3-mm-diameter biopsy punch, which was then deepened with the dental drill, and finally biopsy punch was re-applied to the thinned bone until the bone was penetrated. Subsequently, double or triple glass coverslips were placed over the brain surface and fixed to the free bone edges using Loctite Superbond and 3M ESPE RelyX cement applied in thin layer all over free skull. A metal headbar was then attached to the dried cement with an additional layer of C&B Superbond dental cement. Once the adhesive had set, the animal was revived using a mixture of nexodal, revertor, and flumazenil (1.2 mg, 2.5 mg, and 2.5 mg/kg body weight, respectively) and

received 0.1–0.15 ml of subcutaneous Ringer's lactate solution to prevent dehydration. The animal remained on a heating pad for an additional 30 minutes, or until awake, before being returned to its cage. Carprofen injections were given intraperitoneally for 5 days post-surgery (0.5 mg/ml, 500 µl).

The calcium sensor molecules were introduced via viral transfection. This procedure was performed similarly, but prior to cranial window implantation, with the distinction that the craniotomy had a diameter of 0.5 mm and was created with dental drill. Following hemostasis, the dura mater was penetrated with an injection needle, and through a borosilicate pipette, 200–300 nl of AAV9.Syn.Flex.GCaMP6f.WPRE.SV40 virus (Penn Vector Core) was injected at a rate of 10-20 nl/s. The pipette remained in place for 10 minutes after the completion of the injection to prevent the injected fluid from surfacing.

3.3 Behavioral tasks

3.3.1 Go/Nogo auditory discrimination task

The mice were deprived of water one day prior to habituation. On the habituation day, they were required to spend 1, then 5, and finally 10 minutes in the training setup, with 30-minute intervals between sessions. After each session, they were given water through a Pasteur pipette. This was followed by the commencement of training according to the protocol. If a 0.5-second-long, 5 kHz complex tone was heard by the mice, a lick was required within a 1- to 3 second period starting from the onset of the tone in order for a reward of approximately 5 µl of water to be received (Hit) 0.5 seconds after triggering it. If the lick was missed, no water was given (Miss). However, if a lick was made in response to a different sound (0.5 kHz complex tone), a mild, blinking-inducing air puff was delivered to their face (False Alarm, FA), but if licking was refrained from, no consequences followed (Correct Rejection, CR). A training session lasted for 100-200 trials, depending on the mice's thirst level. Since the reward and punishment were delivered 0.5 second after a variable reaction time period, the symbols indicating the sound on the figures always represent an approximate tone onset, calculated based on the average reaction time (reaction time = time elapsed between tone onset and the first lick

after tone onset). Licking was detected by an infrared sensor. The behavioral protocols were written in Matlab and controlled by Bpod device (Sanworks). The sounds were generated by PulsePal device (Sanworks) and Logitech speakers. Water and air puffs were dispensed by two Neptune electromagnetic valves.

3.3.2 Pavlovian task

In the Pavlovian task, the animals were exposed to two types of sounds: upward and downward chirps lasting 0.5 seconds (from 4 kHz to 20 kHz and vice versa). Following the upward chirp (cue A), a reward was delivered after a 2 second delay in 80% of the cases. No event followed the downward chirp (cue B). In 20% of the trials, no sound was played, and the mice received an uncued reward. There was no application of punishment in this task.

3.4 2-photon imaging system

The imaging system was based on the microscope architecture published by Szalay et al. in 2016. As light sources, MaiTai HP (SpectraPhysics) or a Coherent Chameleon Ultra II (Coherent) lasers were utilized at a wavelength of 920 nm. The emitted beam traversed a complex optical path to reach the specimen. At its start and a subsequent point, quadrant detector sensors and motorized mirrors in a stabilizer compensated for displacements caused by temperature fluctuations of the optical elements. After employing dispersion compensation (4DBCU unit) for optimal signal-to-noise ratio (SNR) and contrast, the laser beam entered the first pair of acousto-optical deflectors. Here, a chirped sinusoidal wave emitted by a piezoelectric controller modulated grid constant of the the crystal, determining the beam's path. The second pair of deflectors compensated for lateral drift occurring during passage through the first, and with only partial compensation, allowed for directing the beam along arbitrarily oriented lines, facilitating point, line, and area scanning (3D chessboard scanning). The sample was illuminated through a 20x magnification objective lens (XLUMPlanFI20×/1.0, water immersion, Olympus), with

ultrasound gel positioned in between. The reflected fluorescent light from the sample was collected using GaAsP photomultipliers (H10770PA-40, Hamamatsu) after isolation from the excitation beam using infrared filters (ET700sp-2p8, Chroma Technology) and dichroic mirrors (700dcrxu, Chroma Technology) with a 700 nm cutoff. A dichroic mirror with a 600 nm cutoff (t600lpxr, Chroma Technology) separated the green and red channels, further supplemented with filters (ET520/60m, ET650/100m, Chroma Technology).

3.5 Imaging of sparsely labeled interneuron population

The measurement procedure was as follows: initially, I created a z-stack within a volume of approximately half a cubic millimeter (maximum: 689 µm × 639 µm × 580 µm), taking a layer image every 10 or 20 µm. These images were then added to the background image pool, and the cells to be scanned during the measurement were marked on them. Around the marked centers, a scanning area of 10 µm in size, consisting of 10-20 lines, was set up with a resolution of 0.5-1 pixel/µm. The scanner, instead of traversing the entire volume, jumped from one of these areas to another, performing the scanning. Therefore, 3D chessboard scanning is orders of magnitude faster or can provide better SNR compared to other scanning modes.

$$\left(SNR_{gain}\right)^2 * v_{gain} = \frac{V_{total}}{\sum_{i=1}^{N_{ROI}} V_i} > \frac{1}{1\%*2\%} \sim 5000, \textbf{ Equation S1}$$

Here, SNR_{gain} and v_{gain} denote the relative gains of speed and SNR, v_{total} is the scanning volume, N_{ROI} is the number of ROIs, v_i is the volume of number i. To record the activity of 120 cells from the mentioned volume of 689 µm × 639 µm × 580 µm using point-by-point volume scanning, it would only be possible at a speed of 0.00062 Hz, instead of the current 27.7 Hz (Table 1). If we limited the scanning to the 19 planes where the cells were located, we could achieve 0.00631 Hz. Using another technique with resonant mirrors for laser beam steering, we could achieve 0.16 Hz, boosted to 1 Hz if only the selected planes were measured. However, this is still a slow speed for in vivo behavioral measurements.

Therefore, for recording such a number of cells from this volume, chessboard scanning is the appropriate choice.

Table 1. Comparison of multiple imaging methods (55).

	schematic of the method	name of the method	calculation of scanning speed	$T_{measurement}$ ($v_{measurement}$)	$V_{measurement}$ compared to chessboard scanning	ratio of collected photons compared to chessboard scanning (SNR^2)	$SNR^2 \times v_{gain}$ compared to chessboard scanning
AO SCANNING	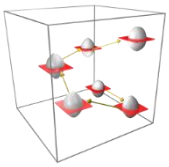	3D AO chessboard scanning	$N_{cell} \times N_{line} \times T_{pixel}$	0.036 s (27.7 Hz)	1	1	1
	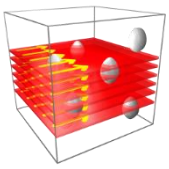	AO point by point scanning of the entire volume	$x \times y \times z \times T_{pixel}$	1611.5 s (0.0006 Hz)	1/44762	1	1/44762
	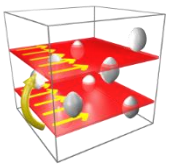	AO point by point scanning in layers containing cell somatas (19 layers)	$x \times y \times N_z \times T_{pixel}$	158.4 s (0.00631 Hz)	1/4399	1	1/4399
RESONANT SCANNING	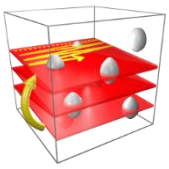	Volume scanning with resonant mirror	$x \times y \times z \times T'_{pixel}$	6.1 s (0.16 Hz)	1/170	1/244	1/41506
	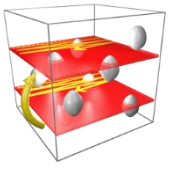	Multiple-layer scanning with resonant mirror and piezo (19 layers)	$x \times y \times N_z \times T'_{pixel}$	0.98 s (1.04 Hz)	1/27	1/244	1/6654

Used parameters:
N_{cell} = 120 (120 cells) x = 548 pixel, y = 507 pixel, z = 193 pixel (total scanning volume was: x = 689 µm, y = 639 µm, z = 580 µm)
N_z=19 (19 z layers were used in volume scanning)

T'_{pixel} = 0.11 µs, (pixel dwell time of resonant scanning, according to a f=16 kHz frequency and the x=548-pixel line resolution of the resonant scanner)
T_{pixel} = 30 µs, (AO pixel dwell time)
N_{line}= 10 (number of lines used to form a frame in chessboard scanning)

3.6 Visual stimulation

An LCD monitor was positioned in front of the contralateral eye of the animal, displaying black and white bars that remained still for 1 second, moved for 6 seconds, and then became still again for another second. The display was gray during inter-trial intervals. The bars appeared at a speed of 1 cycle/s, with 8 orientations at 45° intervals. The gratings were repeated 10 times in a pseudorandom sequence. The software for administering the visual stimulation was written in Matlab.

The orientation and direction selectivity were calculated using the following formulas: $OSI = (Rpref - Rortho)/(Rpref + Rortho)$, $DSI = (Rpref - Ropp)/(Rpref + Ropp)$ (orientation and direction selectivity, (55)). In these formulas, 'pref' refers to the preferred orientation or direction, 'ortho' to the orthogonal orientation, and 'opp' to the opposite direction.

3.7 Data analysis

The control of the microscope, motion correction, calculations related to fluorescence curves, and partially the data representation were executed using the Matlab-based MES software (Femtonics). ΔF/F values were calculated at the beginning of the recordings, followed by establishing a new baseline during the 2-second period preceding the tone onset. Determining whether a neuron was activated by an event was based on changes in fluorescence within the 2-second duration post-event. Artifacts not removed by motion correction were eliminated through partial Gaussian filtering and interpolation. In the analysis of reliability (the proportion of trials in a given trial type in which a cell was active) and synchronicity (the number of cells activated simultaneously in a trial), a neuron in a particular trial was considered active if the average value within a 250 ms range around the peak ΔF/F exceeded 2 SDs. The identification of responsive neurons to a specific event at the session level was done using a t-test.

For the investigation of heterogeneity, I employed linear regression. In one case, the exploratory variable was the hit rate, while in the other, the four functional brain regions (motor, somatosensory, parietal and visual cortices) were used as categorical variables with dummy coding. The dependent variable was the magnitude of the average response of the VIP interneuron population to the tone component relative to the reward component.

PCA for examining cell-level heterogeneity was conducted on cells with a positive reward response, excluding 16 due to low SNR. The data were standardized, followed by further normalization using the maximum value of the 0-4 second post-reward period. The PCA was run for the same period.

3.8 Generalized linear model

To investigate the individual contributions of arousal, locomotion, and reinforcement to the function of VIP interneurons, I built a generalized linear model, where the explanatory variables included movement velocity, tone, water and air puff events, and pupil diameter. The events were modeled using Gaussian kernels or derivatives thereof (for water: Gaussian + linear fit until the timepoint when the mice consistently maintained high licking activity). After standardization, a lasso regularized regression was used with automated hyperparameter tuning and five-fold cross-validation.

3.9 Recording pupil diameter & locomotion

Pupil videos were captured using a CMOS camera (Basler puA 1600–60 µm) mounted with a 4x objective lens. Following thresholding, an ellipse was fitted to the pupil, with its largest diameter used for further analysis. After Gaussian filtering, artifacts caused by blinking were manually interpolated. Subsequently, the curves obtained based on the formula $\Delta P/P_0 = (P(t)-P_0)/P_0$ were divided into low and high arousal groups, based on the area under the curve, where P(t) denotes the pupil diameter over time, and P_0 represents

baseline pupil diameter. The speed of the disc on which the animals ran was measured using an optical mouse (Urage reaper 3090, Hama).

3.10 Statistics

All statistics were performed using Student's t-test unless it is otherwise indicated. To evaluate normality of the data, Lilliefors test was applied that showed that in 78% of VIP interneurons the reinforcement-related responses followed normal distribution. '*' symbols used in the figures mean different levels of significance as $*p < 0.05$, $**p < 0.01$, $***p < 0.001$.

4. Results

4.1 Behavioral task

In a subset of the experiments, I employed an auditory discrimination task in which animals were required to lick in response to a specific sound to receive a water reward and withhold licking following another sound to avoid a mild air puff punishment (Go/Nogo task). This task was learned over 3 ± 0.6 (mean ± SD) sessions, with the animals achieving more than 80% correct responses. Measurements were conducted during the training phase, when the animals still triggered a substantial number of punishments. The Hit and FA rates were 51±4% and 41±4%, respectively (n=18 measurement sessions from 16 animals, $p<0.01$, t-test, **Figure 4**). In another series of experiments, the animals were presented with two sounds, one of which was consistently followed by an automatic water reward. Additionally, in some trials, they received an uncued reward (Pavlovian task). Measurements were taken after 10 sessions, by which time the animals could distinguish which sound was followed by water (55).

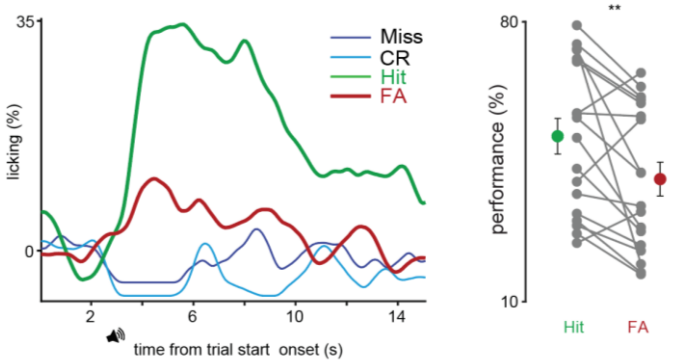

Figure 4. Behavioral performance data of the mice used in the study (original figure).

Left, average licking traces from an example measurement session for Hit (thick green), FA (thick red), Miss (thin dark blue) and CR (thin light blue). Speaker icon marks the tone onset. Right, performance of n=16 animals during the 2-photon measurement sessions.

4.2 Scanning sparse VIP interneuron population

VIP interneurons are characterized by comprising only about 10-15% of all cortical inhibitory cells, representing a sparse interneuron population (56). Additionally, their cell bodies are smaller in size, attributes that do not lend themselves well to addressing the questions posed in our objectives using electrophysiological tools. Therefore, I employed 2-photon microscopy capable of three-dimensional imaging (57-59), utilizing a 3D chessboard scanning mode (59). In this approach, the scanning laser beam traces lines in a plane around coordinates designated based on the spatial position of the cells, scanning the cells and their immediate surroundings before jumping over the interspersed space to begin scanning the next cell (**Figure 5A**). This method enabled us to achieve a 170-fold increase in speed and a 15-fold improvement in signal-to-noise ratio (SNR) compared to resonant mirror-based systems (**Table 1**). This allowed us to simultaneously measure the activity of up to 120 cells at a speed of 27.8 Hz from a volume of 689 µm × 639 µm × 580 µm (**Figure 5B**) (55).

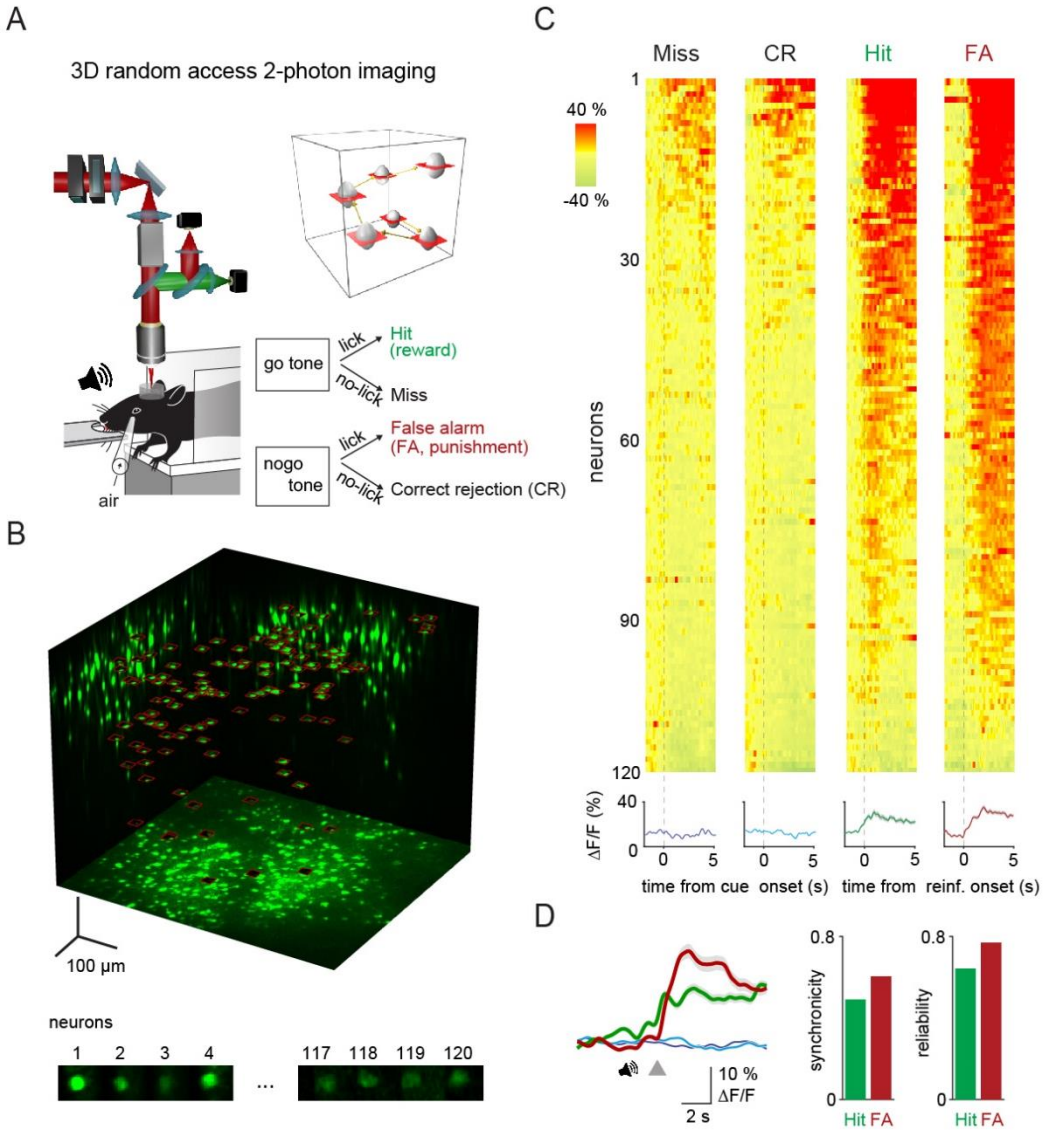

Figure 5. 3D-random-access 2-photon imaging of VIP interneurons in an auditory discrimination task (55).

A) *Schematic of the combined fast 3D AO imaging and behavior experiments. Head-restrained mice were trained to perform a sensory discrimination, an auditory Go/Nogo task during 3D AO imaging using the chessboard scanning method (inset).*

B) *Top, maximal intensity z and two side projections of the GCaMP6f-labeled VIP interneuron population imaged by fast 3D AO scanning in the MPta. All 120 neurons within the cubature were simultaneously imaged using 120 frames of chessboard scanning (red frames). Bottom, exemplified image frames of chessboard scanning. Frames of chessboard scanning capture not only somata of the neurons but also the*

surrounding background information. In this way, fluorescence information is preserved during brain motion in behaving animals for motion correction.

C) *Top, somatic Ca^{2+} responses recorded in the MPta during example Miss, CR (Correct Rejection), Hit, and FA (False Alarm) trials were aligned to the reward and punishment onset, and for Miss and CR trials, to the cue onset. Responses were ordered according to their maximum amplitude. Bottom, mean ± SEM responses.*

D) *Left, average transients of a measurement session (128 trials) for Hit (thick green), FA (thick red), Miss (thin dark blue) and CR (thin light blue) responses recorded from the 120 VIP interneurons. Grey triangle marks the reinforcement onset in case of Hit and FA. Averages of Miss and CR trials were aligned according to the expected reinforcement delivery calculated based on the average reaction time. Right, average synchronicity (mean ± SEM) and trial-to-trial repeatability (reliability) of the individual neuronal responses.*

For three-dimensional measurements, some employ point-by-point acousto-optical scanning, but this approach is not practical for behaving animals. Even with the best surgical techniques, one can expect motion artifacts of approximately 3 μm. Therefore, during the measurements, it was necessary to capture a small part of the intercellular region surrounding the VIP interneurons, which does not contain information relevant to us, for later offline motion correction. The use of this correction is critical for the accurate extraction of data (59).

4.3 Scanning sparse PV interneuron population

Using the AO microscope with chesboard scanning, we were able to measure the activity of various interneurons during physiologically relevant brain events (60). In the experimental setup shown in **Figure 6**, a water-deprived animal received spontaneous water delivery controlled by the BPOD system. During these periods, the probability of sharp-wave ripple events increased, during which neuronal activity was recorded. Subsequently, dendritic calcium transients were detected in the active cells using ribbon scanning. The primary aim of this project was to uncover the calcium dynamics of PV

interneurons in the hippocampus during memory formation. While the biological findings are not detailed here, this experiment serves as a clear demonstration of the imaging system's utility in capturing sparse interneuronal activity.

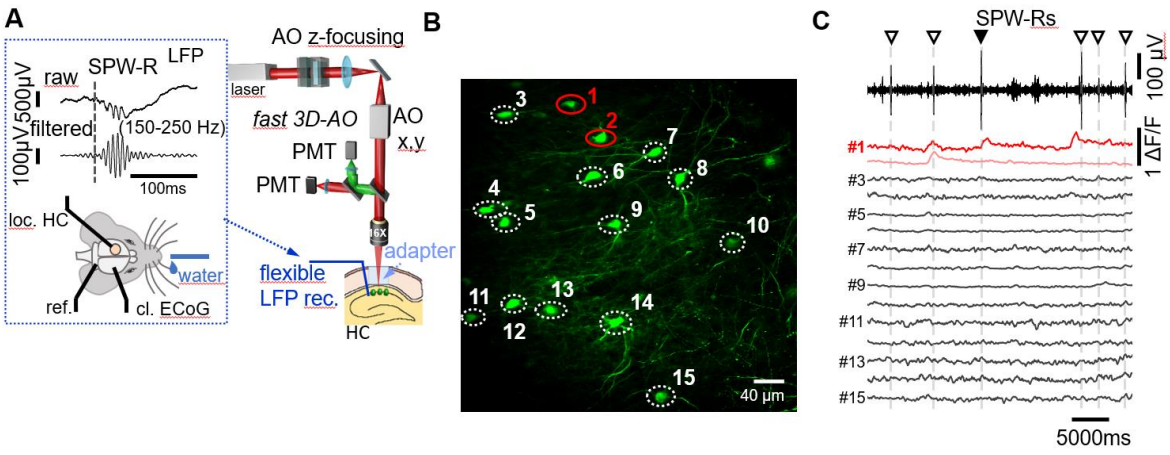

Figure 6. 3D-random-access 2-photon imaging of PV interneurons during sharp-wave ripple events in the hippocampus (60).

A) *Experimental setup illustrating the simultaneous electrophysiological and optical recording of hippocampal neuronal activity during sharp-wave ripple (SWR) events.*

B) *Overview image showing PV interneurons in the hippocampal region.*

C) *Simultaneously recorded local field potential (top trace) and calcium responses (bottom) of PV interneurons during SWR activity.*

4.4 Reinforcement activates VIP interneurons in the neocortex

The measurements commenced in the medial parietal cortex (mPTA), an associative area linked to the visual system. In this region, a small subset of VIP interneurons was activated during Miss (no lick for Go sound) and Correct Rejection (CR, no lick for NoGo sound) trials (**Figure 5C**). Conversely, during Hit (reward) and False Alarm (FA, punishment) trials, 85 and 90% of these cells were activated with high reliability (64 and 77% respectively) and synchronicity (49 and 60%) (**Figure 5C-D**). In contrast, PV interneurons did not exhibit population-level homogenous activation following reward

and punishment (29 and 10% in n=2 mice, **Figure 7**). As fiber photometry from auditory cortex also did not show any significant activation after reward delivery, PV cells were left out from further measurements and analysis (55).

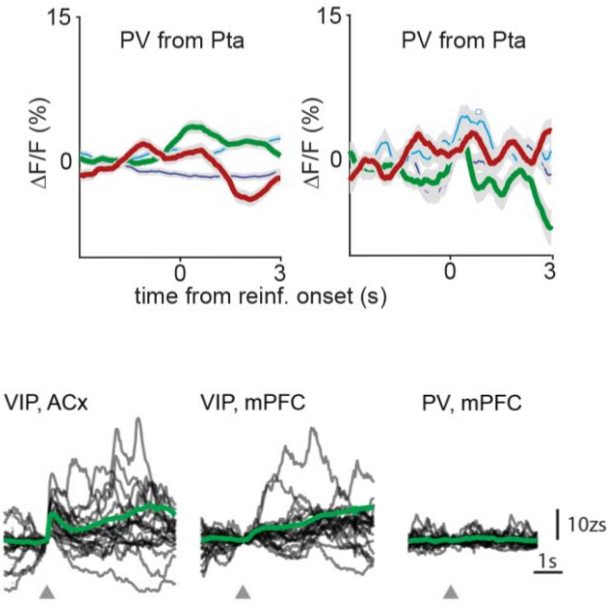

Figure 7. Parvalbumin-containing interneurons do not respond to reinforcement (55).

Top, Average transients of PV interneurons (mean ± SEM of n=17 and n=37 cells) for Hit (thick green), FA (thick red), Miss (dark blue) and CR (light blue) recorded from the parietal cortex.

Bottom, Fiber photometry measurements from the auditory cortex (ACx) and the medial prefrontal cortex (mPFC) during uncued reward delivery (triangles). Black traces: individual trials, green traces: session averages.

Subsequently, I extended the measurements to cover several areas of the dorsal cortex (motor, somatosensory, parietal, visual), recording the activity of 811 VIP interneurons from these regions (n=16 mice, n=18 injection sites). Between 83 and 85% responded to

reward and punishment, and 15% to auditory cues in Miss and CR trials (**Figure 8A-D**). A strong correlation was observed between the amplitudes of responses to reward and punishment (R=0.73, **Figure 8E**).

Thus, across all examined brain regions, we found recruitment of the majority of VIP interneurons related to reinforcement. Our collaborators observed similar results in the mPFC and auditory cortex using fiber photometry (**Figure 8A**) (55).

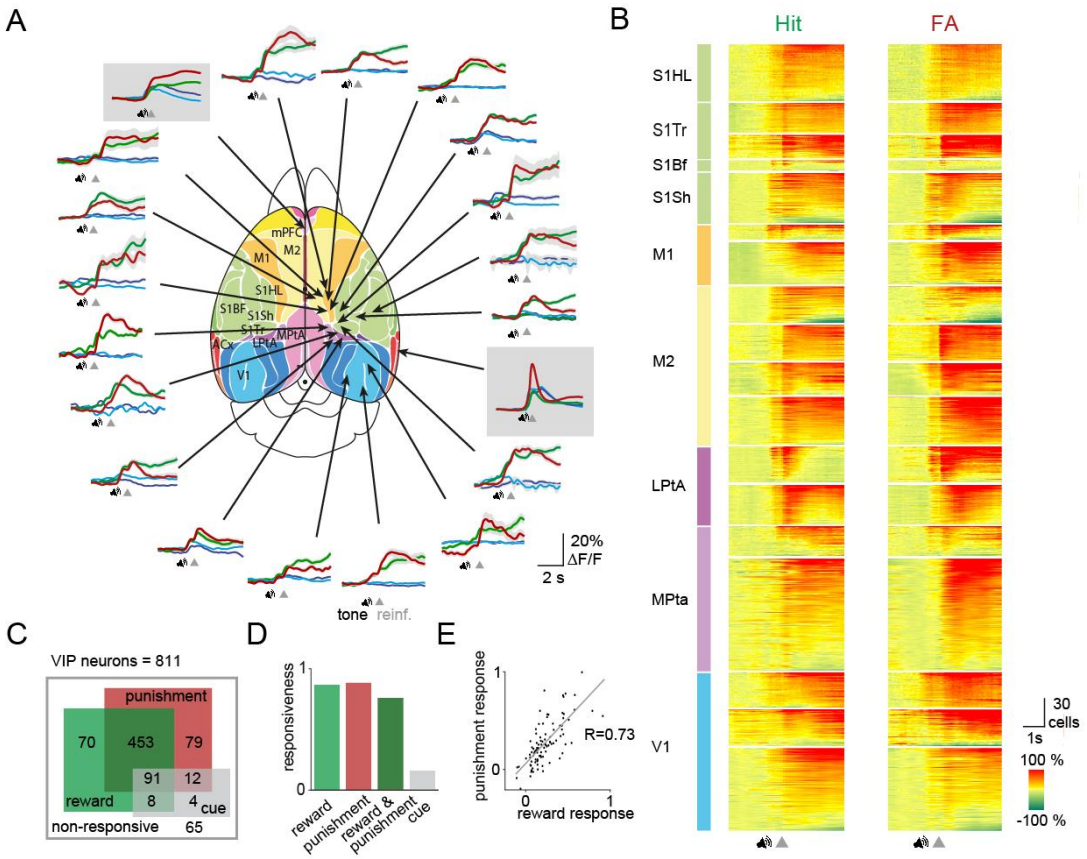

Figure 8. Reward and punishment recruit VIP neuronal activity across the dorsal cortex (55).

A) *Ca^{2+} responses of individual VIP interneurons recorded separately from 18 different cortical regions from 16 mice with fast 3D AO imaging were averaged for Hit (thick green), FA (thick red), Miss (dark blue), CR (light blue). Fiber photometry data were recorded simultaneously from mPFC and ACx regions and are shown in gray boxes.*

Functional map (61) used with the permission of the publisher. Speaker symbols represent the average time of tone onset, and grey triangles mark the reinforcement onset in case of Hit and FA. Averages of Miss and CR trials were aligned according to the expected reinforcement delivery calculated on the basis of the average reaction time. mPFC: medial prefrontal cortex, ACx: auditory cortex, S1Hl/S1Tr/S1Bf/S1Sh: primary somatosensory cortex, hindlimb/trunk/barrel field/shoulder region M1/M2: primary/secondary motor cortex, Mpta/Lpta: medial/lateral parietal cortex, V1: primary visual cortex.

B) *Each line of the raster plots shows average neuronal response for Hit and FA. Abbreviations indicate color coded cortical recording positions shown in panel A. Speaker symbol represents the approximate time of tone onset, as reaction times of the animals could be different. Responses were normalized in each region and ordered according to their maximum amplitude.*

C) *Responsiveness of 811 VIP interneurons for Hit and FA.*

D) *Bar chart of data from C.*

E) *Average response of individual VIP interneurons for FA as a function of the response for Hit. Note the high correlation (R=0.73).*

4.5 Heterogeneity in the reinforcement response of VIP interneurons

Heterogeneity was observed both at the cellular level and across sessions, therefore I compared the measures of neuron-to-neuron and inter-individual variance. To do this, I utilized the coefficient of variation (CV=SD/mean) calculated from the average responses of cells and sessions measured in the PTA (n=4 mice, n=236 cells, **Figure 9**). The CV was computed separately for each trial type: the cell-to-cell CV was similar across all types (Miss: 0.80, CR: 0.70, Hit: 0.57, FA: 0.58), and the inter-individual CV was also comparable in Miss and CR, but significantly lower in Hit and FA trials (Miss: 0.94, CR: 0.69, Hit: 0.25, FA: 0.20). This indicates that in cases of reinforcement, inter-individual differences were much smaller, with the variance being more pronounced at the level of individual cells (55).

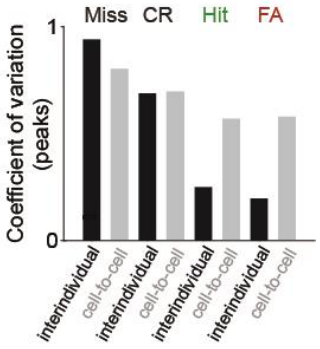

Figure 9. Comparison of inter-individual and cell-to-cell variability in the four trial types (55).

4.6 Cell-to-cell variance

The variance in the cellular-level response to reinforcement was assessed by analyzing the neurons that were activated during Hit trials. We conducted a principal component analysis (PCA) on the average responses of these neurons, followed by k-means clustering (n=606 cells, **Figure 10**). These methods facilitated the identification of five distinct functional groups. It's important to note that these groups differed primarily in the late phase of their fluorescence curves, while their tone and reward-related components were similar. Consequently, we categorized the resulting clusters as 'fast' (n=109), 'delayed' (n=88), 'sustained' (n=177), 'biphasic' (n=120), and 'slow' (n=112). The distribution of these groups varied across functional areas, with the 'fast' group predominantly present in the PTA and the 'slow' group more in V1 ('fast' mean ΔPta-V1=3.22, Mann-Whitney test, $p=3.77\times10^{-9}$; 'slow' mean ΔPta-V1=−7.79, $p=3.77\times10^{-9}$). However, no differences in distribution were observed based on cortical depth (55).

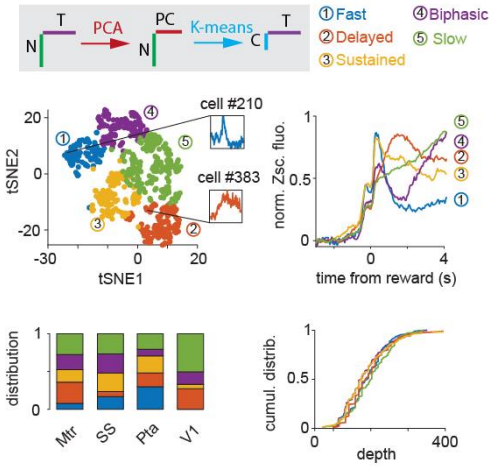

Figure 10. Cellular-level variability in the reward response of VIP interneurons (55).

Upper left, T-distributed Stochastic Neighbor Embedding (tSNE) plot of the reward mediated activity of VIP interneurons after PCA. Individual neurons are color coded according to their cluster type obtained using a k–means clustering algorithm. Inserts show the average response of single rapidly (blue) or delayed (orange) activated VIP

interneurons. Right, average GCaMP6f responses from different clusters of VIP interneurons after reward delivery. N: number of neurons, T: time, PC: principal components, C: clusters.
Lower left, distribution of the clusters across different cortical areas (Mtr: motor cortex, SS: somatosensory cortex, Pta: parietal cortex, V1: primary visual cortex). Right, cumulative distribution of the clusters shown as a function of cortical depth.

It is conceivable that these clusters may reflect the diverse receptor compositions, ion channel makeup, and connectivity of different VIP interneuron subtypes. Therefore, in part of the measurements, I determined the average somatic diameter of the cells (full width at half maximum [FWHM]). Both at the level of individual mice (7/8) and collectively, a bimodal distribution was observed (**Figure 11A**). There was no difference in the diameters of reward and punishment responsive and non-responsive cells (Hit: 10.0 ± 0.1 vs 9.9 ± 0.1 µm, p=0.39; FA: 10.3 ± 0.2 vs 9.8 ± 0.1 µm, p=0.07, Mann-Whitney test, **Figure 11B**), but there were differences between the PCA-identified groups, with the 'fast' and 'sustained' neurons having the largest somata (fast: 10.2 ± 0.4 µm, delayed: 9.8 ± 0.2 µm, sustained: 10.4 ± 0.2 µm, biphasic: 10.0 ± 0.2 µm, slow: 9.4 ± 0.2 µm, H=14.8, p=0.005, Kruskal-Wallis H-test, **Figure 11C**). This result supports the hypothesis that the functional groups identified by PCA may also differ anatomically and represent distinct VIP interneuron subtypes (55).

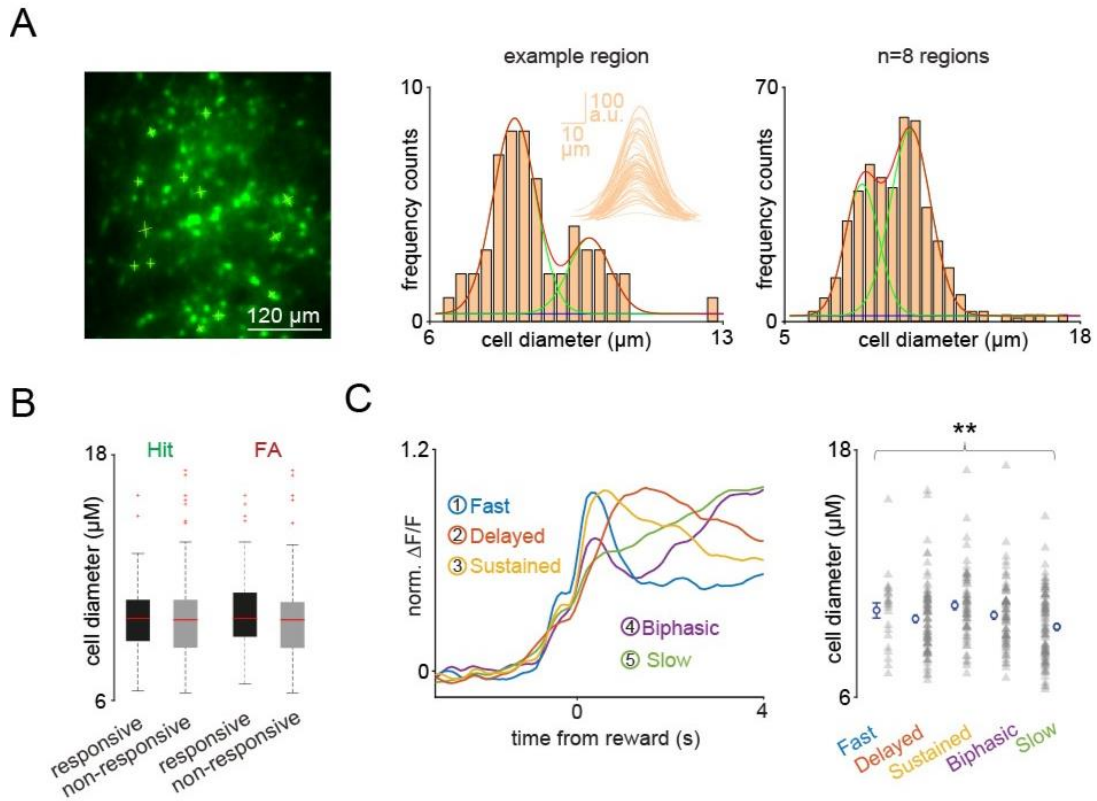

Figure 11. Cell diameter distribution of the recorded VIP interneuron population and its relation to the activity (55).

A) *Left, maximal intensity projection of the GCaMP6f-labeled VIP interneuron population imaged by fast 3D AO scanning in one of the sessions. Thin yellow lines symbolize the lines used to determine the fluorescence profile of the somata. Middle, cell diameter distribution of an example region. Inset: Averaged cross-section fluorescence profiles of the somata for FWHM calculation. Right, cell diameter distribution of the n=8 mice that were used for this analysis.*

B) *Box-and-whisker plots of the cell diameter of Hit and FA responsive and non-responsive cells. Median, 25th and 75th percentiles, range of nonoutliers and outliers are depicted.*

C) *Left, average GCaMP6f responses of the VIP interneurons after reward delivery separated into clusters by PCA. Right, variability in the cell diameter of the clusters. Asterisks mark significant differences between the means of the groups.*

4.7 Reward expectation modulates reinforcement-related recruitment

The session-to-session variance was characterized by the relative magnitude of the cue-related response component compared to the reward signal. Interestingly, this was not influenced by the functional region where the recording had happened (somatosensory, motor, visual, or PTA, R^2=18.2%; p=0.41). However, it was affected by the number of times the animal correctly licked to trigger reward following a Go cue during the session (hit rate = number of Hit trials / number of Go trials). The hit rate showed a direct correlation with the amplitude of the cue response (R^2=39.0%; p=0.006, **Figure 12A**). Additionally, in some animals, the large reward-related response component seen at the beginning of the imaging session diminished by the end, with the cue-related component becoming dominant (reward/cue ΔF/F early 1.3+/-0.3 vs late 0.7+/-0.1, p=0.02, **Figure 12B**). This was only observed in animals where the hit rate was greater than 50% throughout the session, interpreted as an indication that they had learned to trigger the water reward by licking (55).

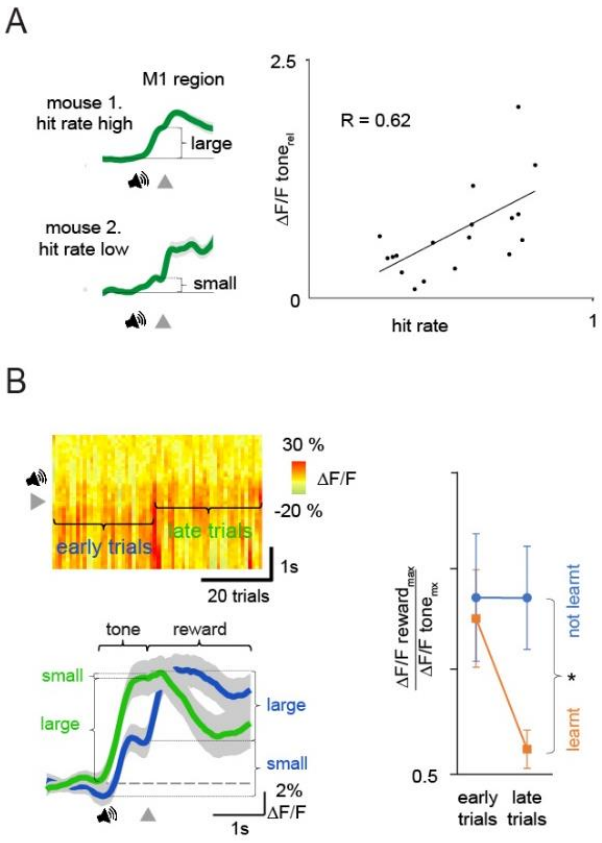

Figure 12. Heterogeneity in VIP neuronal responses across the dorsal cortex (55).

A) *Heterogeneity of the cue responses. Left, higher hit rate was associated with larger tone-related response components in the population average traces of Hit trials. Right, scatter plot of the size of the average tone response and the hit rate.*

B) *Changes of the cue and reward related response-components. Top left, each vertical line of the raster plot show the average population response in Hit trials. Average fluorescence responses from early and late trials as highlighted in top of panel B. Right, reward/cue response ratio in case of animals that learned or not learned the task during the session in early and late trials.*

The results from Go/NoGo task suggested that the mice potentially acquired the task during the imaging session, with the neurophysiological manifestation of this learning depicted in **Figure 12**. To investigate this phenomenon in more detail, I trained the mice for a minimum of 10 days on the simpler Pavlovian task and then measured the activity of the VIP interneurons in the mPTA. In this task the mice did not have to lick to receive

water, but when they learned to associate the correct cue with consecutive rewards, anticipatory licking was observed, the extent of which served as a measure of behavioral performance. Water was delivered following cue A but not cue B, and in some trials, an uncued reward was also given. Two observations emerged from the results: cue A elicited a stronger signal than cue B (5 vs 1%, $p<0.001$, n=3 mice n=153 neurons, **Figure 13B**), and the uncued reward signal was greater than the cued reward (6 vs 3%, $p<0.001$, **Figure 13B**). I concluded that if the animal anticipated the reward, the reward itself did not trigger as strong an activation, but the representation of the predictive cue was reinforced, very similar to what has been observed in the dopaminergic system (7).

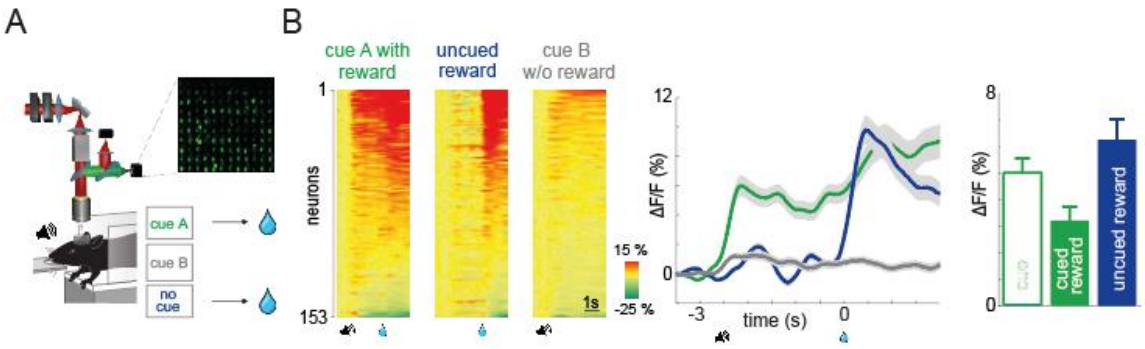

Figure 13. VIP neuronal responses reflect reward expectation (original figure).

A) *Schematic of the behavior experiments combined with fast 3D AO microscopy.*

B) *Left, lines of raster plots show the average neuronal response in different trial types (cue A with reward, uncued reward, cue B without reward). Responses were ordered according to their maximum amplitude. Cue onset is represented by speaker symbols, water drop shows the time of reinforcement. Middle, average Ca^{2+} responses of VIP interneuron population from 3 sessions. Right, bar charts of the data for cue A, cued reward, and uncued reward. (mean ± SEM).*

4.8 Dissecting reinforcement, arousal and motion related activity of the VIP interneurons

The presumed functions of VIP interneurons include transmitting information about locomotion and arousal states (44, 62, 63). Therefore, we investigated the extent to which these functions could be distinguished from reinforcement signaling. While the animals performed the Go/NoGo task, they ran on a disc whose speed was recorded, and their pupil dilation was tracked using a camera, reflecting the brain's arousal level (**Figure 14A**). Hit and FA trial types were divided into low and high arousal trials based on pupil dilation. VIP interneuron activity showed a positive correlation with pupil diameter (median correlation coefficient 0.31, **Figure 14B**). Neurons with both higher and lower correlation coefficients responded to reinforcement, but those with higher correlations maintained their activity thereafter. Averaging fluorescence curves for trials with high and low arousal changes, from both the somatosensory and motor cortices, as well as using fiber photometry in the mPFC, showed that VIP interneuron responses were modulated by arousal level; lower arousal corresponded to reduced fluorescence signals, and higher arousal to increased signals (somatosensory cortex: large vs small pupil $\Delta F/F$: 40 vs 29% n=26 cells, t-test, p=0.01; motor cortex: large vs small pupil $\Delta F/F$: 28 vs 18%, n=111 cells, $p<0.001$; mPFC: large vs small pupil $\Delta F/F$: 3.8 vs 1.4%, n=6 mice, p=0.01, **Figures 14C-E**). However, it is noteworthy that despite a ~5-fold difference in pupil diameter, only a ~1.5-fold difference was observed in the fluorescence signal, suggesting that the reinforcement-associated response cannot be simply attributed to changes in arousal. When examining the modulatory effect of locomotion, similar results were obtained: modulation was observed in the responses to reinforcement in trials with both high and low locomotion speed (average speed change for the two groups: 1.20 cm/s vs –0.23 cm/s) following reinforcement (somatosensory cortex: high vs low speed change $\Delta F/F$: 42 vs 27% n=26, t-test, $p<0.001$; motor cortex: high vs low speed change $\Delta F/F$: 30 vs 19%, n=86, $p<0.001$; mPFC: high vs low speed change $\Delta F/F$: 5 vs 3.5%, p=0.02, **Figures 14F-H**). At the level of individual cells, the correlation between movement and activity was lower than that observed for arousal (median correlation coefficient, 0.11) (55). Interestingly, in the auditory cortex, neither arousal nor movement-induced modulation was observed (data not shown). This could be due to a phenomenon termed

'tone-related network suppression,' mediated by SOM interneurons (64), or possibly due to 'movement-induced suppression' also observed in this cortex (65).

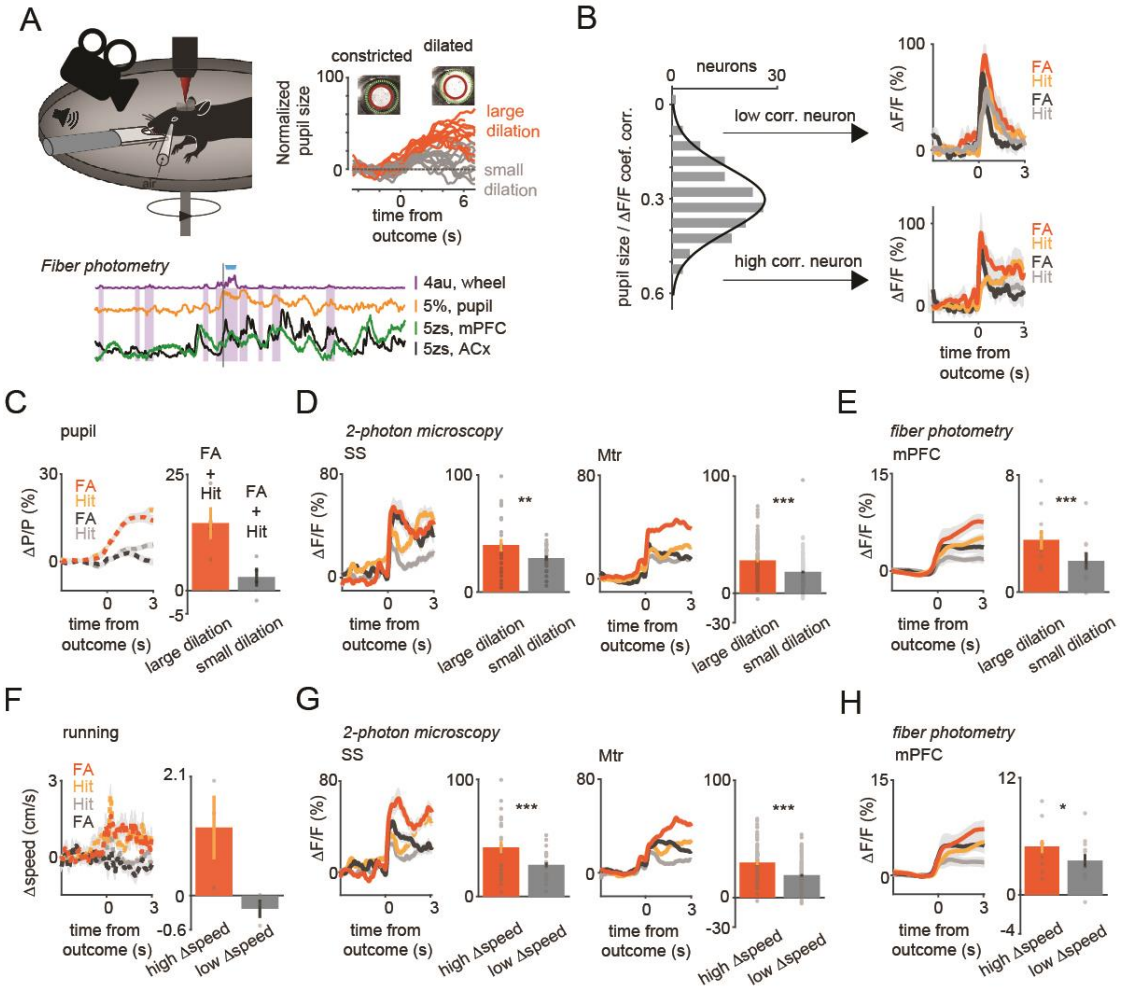

Figure 14. Arousal states modulate VIP neural responses to sensory cues and reinforcers (55).

A) *Upper left, schematic of measurements. Pupil and movement were simultaneously monitored during 3D imaging in the auditory Go/NoGo task. Upper right, high (orange) and low (gray) arousal states were separated by changes in pupil diameter. Below, 60 sec continuous monitoring of different behavioral variables together with VIP interneuron population activity in ACx and mPFC. The black bar indicates the timing of an uncued reward delivery. Blue triangles indicate licking events. Purple shaded boxes represent running bouts.*

B) *Left, distribution of correlation coefficients of relative change in pupil diameter (ΔP/P) and VIP neuronal response. Right, reinforcement-associated responses were significantly larger when relative change in pupil diameter (ΔP/P) was higher during the task. Red and orange indicate FA and Hit responses associated with higher ΔP/P. FA and Hit responses associated with low ΔP/P are in black and gray, respectively.*

C) *Average pupil dilation traces during high (red and orange) and low (black and gray) pupil changes for FA and Hit trials for SS and Mtr recordings in panel D. Bars indicate average amplitudes (mean±SEM, Hit and FA combined).*

D) *Population averages for Hit and FA during high and low pupil change in the SS and Mtr regions. Bars indicate average amplitudes (mean±SEM, Hit and FA combined). Even in the late period, when the outcome responses were dissipated, larger changes in pupil diameter at the time of reinforcement were associated with higher VIP responses.*

E) *Same as D but for fiber photometry in the mPFC.*

F) *Same as C but for running speed.*

G) *Same as D but for running speed.*

H) *Same as E but for running speed. Higher relative change in the running speed was associated with larger neuronal responses recorded with 3D imaging or fiber photometry.*

Finally, to estimate the contributions of arousal, locomotion, and reinforcement to the activity of VIP interneurons, I created a generalized linear model (**Figure 15**). The model was capable of explaining 18.8 ± 11.1% of the variance in the fluorescence curves derived from the motor and somatosensory cortices. The best predictor was the pupil diameter, followed by reward, punishment, locomotion, and tone (weights = 0.055, 0.031, 0.028, 0.020, 0.018 respectively; tone was not significant, but for the rest $p<0.001$). This analysis supports the hypothesis that locomotor activity and arousal itself are not entirely sufficient to explain the activity of VIP interneurons (55).

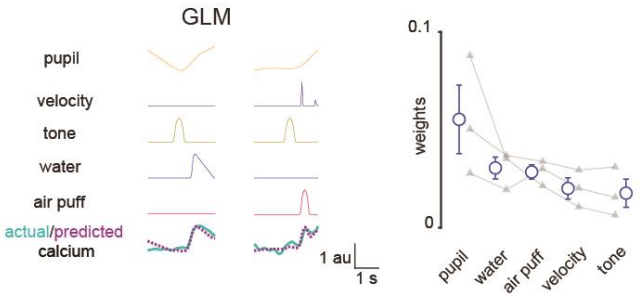

Figure 15. Arousal, reinforcement and movement explain VIP neural activity (55).

Left, actual calcium signal, explanatory variables, and predicted calcium from a generalized linear model that was built to assess distinct contributions of arousal, reinforcement, cue, and motor events. Right, weights of the explanatory variables in the model.

4.9 VIP interneurons in the local sensory processing

As part of cortical microcircuits, VIP interneurons, similar to other cell types, participate in sensory processing based on input characteristic to their specific cortical area. Generally, their sensory tuning is weak compared to other cell types (28, 38, 40). In the following series of experiments, I aimed to investigate any potential relationship between the global, reinforcement-related activation mode and their local signal processing. Alongside the previously used Go/NoGo task, I also recorded the sensory responses of VIP interneurons to visual stimulation. To eliminate variance caused by movement, arousal and any other cognitive processes, the animals were lightly anesthetized using isoflurane. For visual stimulation, differently oriented drifting grating bars were used (**Figure 16A**). Individual cells responded, with varying specificity, to one or more orientations (**Figure 16B**). Generally, as consistent with literature, they were more broadly tuned compared to pyramidal cells (**Figure 16C**). The reinforcement response weakly correlated with responses to visual stimuli (Pearson's R value for reward: 0.16, for punishment: 0.23, and reward and punishment combined: 0.22, R^2=0.05, F=8.3, p=0.005, **Figure 16D**), but did not correlate with orientation or direction selectivity (Pearson's R value for OSI: 0.08, p=0.31, for DSI: 0.06, p=0.45). This supports the notion that VIP interneurons can independently participate in both global reinforcement signal transmission and local sensory signal processing (55).

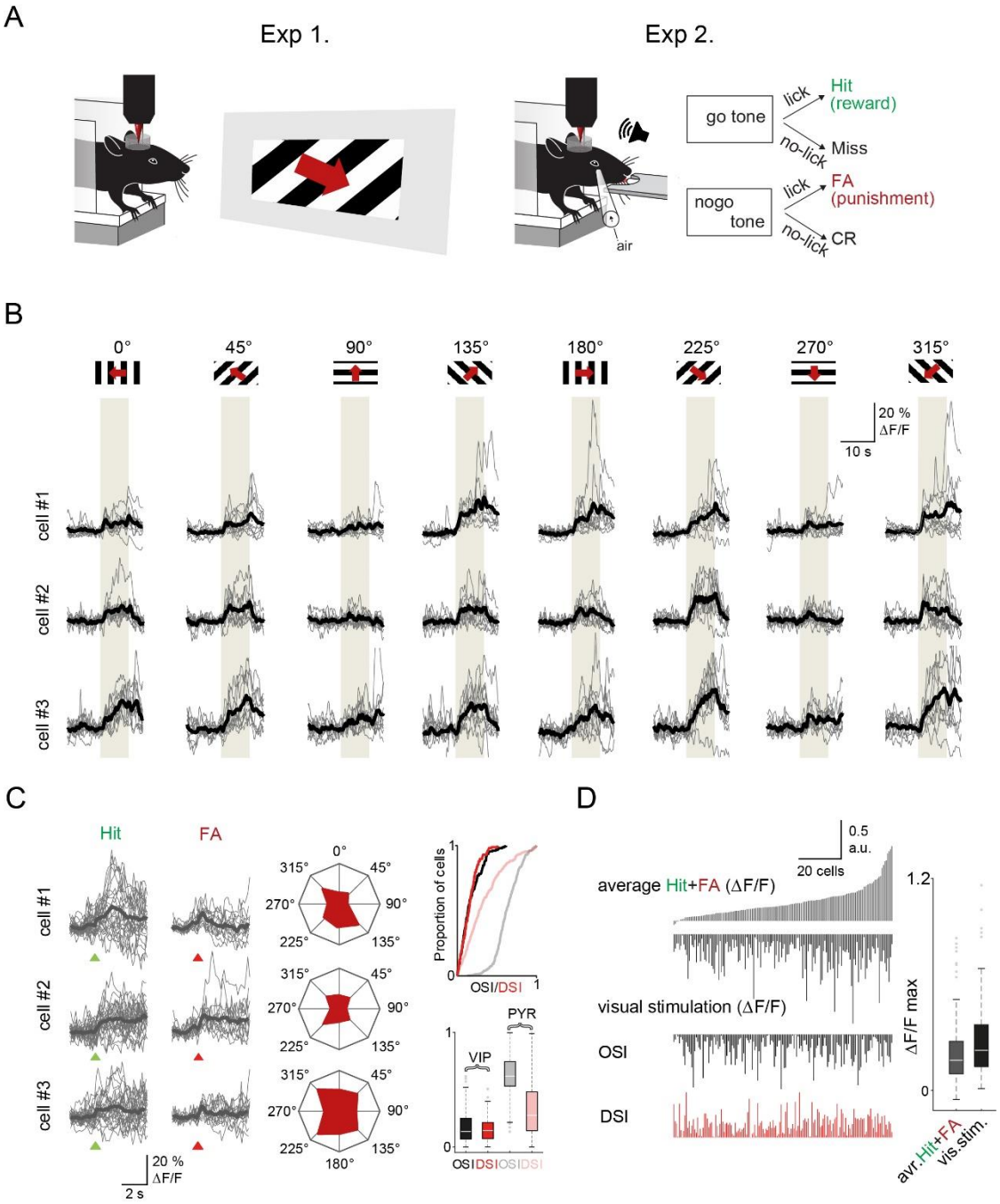

Figure 16. Visual cortical VIP interneurons respond to both visual stimuli and reinforcers (55).

A) *Schematic of the measurement. Orientation tuning was mapped in a first set of experiments (Exp. 1) which was followed by recordings of the same neurons during the auditory Go/NoGo task (Exp. 2). Both set of recordings were performed using fast 3D AO imaging.*

B) *Individual Ca^{2+} responses from three different VIP interneurons to visual stimulation with moving grating in 8 different directions. The grey boxes indicate the duration of the visual stimulation.*

C) *Left, responses of the same three cells to reinforcement. Middle, polar plots of neuronal responses to visual stimulation from the same neurons. Right top, cumulative distribution plot of OSI and DSI parameters of VIP (black and red) and pyramidal cells (gray and pastel red), (VIP: n=157 cells, n=3 mice, pyramidal cells: n=383 cells, n=3 mice). Right bottom, OSI and DSI values of the same cells. Box-and-whisker plots show the median, 25th and 75th percentiles, range of nonoutliers and outliers.*

D) *Correlation between reinforcement and visual responses in the same VIP interneurons (n= 157). Each column refers to a single cell. From top to bottom: mean of the average Hit and FA responses, average visual responses, mean orientation selectivity index (OSI) and mean direction selectivity index (DSI). The cells were ordered according to the amplitude of the averaged reinforcement signal. Right, maximums of reinforcement-related and visual stimulation responses. Box-and-whisker plots show the median, 25th and 75th percentiles, range of nonoutliers and outliers.*

5. Discussion

In this thesis, I presented the concept of predictive processing with two phenomena that are understandable and explainable through this framework. Since reinforcement from the environment is necessary in predictive models for the maximization of rewards, and these calculations presumably occur in the cerebral cortex, it is plausible that information about reinforcement is represented in the cortex. During my experiments, I identified that VIP interneurons conveyed reinforcement signals as global teaching signals in the early stages of training. As the animal adapted its behavior to the task and no longer required this teaching signal, it shifted to the cue, akin to the classical reward signaling described in the dopaminergic system (7). This reinforcement signaling mechanism was not explainable by either the animal's arousal state or the local sensory properties of the cells. The learning-related modulation elucidated why VIP interneuron activity post-reward was not observed in experiments using well-trained animals (40, 42). Therefore, it is considerable to not to call these activations reinforcement signals but reinforcement (reward) prediction error signals (56).

A fundamental question is how the teaching signal appearing on VIP interneurons reaches the cortex. Our own investigations, not detailed here, along with others, have found that cholinergic innervation may be one of the main pathways for signal transmission (66). VIP interneurons can be activated or depolarized by acethylcoline (25, 36, 67). Inhibition of this pathway impaired task performance, and the temporal kinetics of cholinergic activity mirrored that of the VIP interneurons. Its role in reward timing could be related (68). VIP interneurons also have serotonin receptors (35), but their role is not yet clear, although this system also mediates reward-related information (21). The effect of noradrenergic neurotransmission on VIP interneurons is not well characterized. However, the noradrenergic system has an important role in learning (69), likely exerting its effect through pyramidal cells. As noradrenaline acts on metabotropic receptors in the brain (70), its role in millisecond-scale reinforcement signaling may be more modulatory, i.e., strengthening or weakening neurotransmission. The role of the thalamus, from whose posterior medial part axons arrive at the VIP cells eliciting cortical disinhibition (34),

remains a question, although reward-related activity was limited here (71). However, inhibition of this thalamic nucleus during the task reduced learning.

During the investigations, we did not find reinforcement-related activation in PV cells. SOM interneurons were not examined in this study. Since the microcircuit role of VIP interneurons involves disinhibition of pyramidal cells by inhibiting SOM and, to a lesser extent, PV cells, their activity may be responsible for synaptic strengthening related to learning in pyramidal neurons.

The principal component analysis (PCA) results presented here identified functional groups within the VIP interneuron population. Since these groups showed a correlation with an anatomical parameter, the soma diameter, it is conceivable that they represent morphologically and physiologically distinct subpopulations. A comprehensive classification of VIP interneurons in the dorsal cortex considering morphology, connectivity, and neurophysiological parameters, is not yet available. According to some opinions, the VIP interneuron population can be largely non-overlappingly divided into groups based on the expression of calretinin and cholecystokinin (CCK). CCK-positive cells tend to innervate pyramidal cells directly, are morphologically akin to basket cells, and are located closer to the surface of the cortex (72). However, information is lacking on whether there is a difference in the activation profiles of non-CCK-expressing cells. VIP interneuron population predominantly causes disinhibition might be due to the fact that non-CCK, CR-positive VIP interneurons are more numerous (CCK+: 10-30%, CR+: 50-70%), and primarily innervate SOM interneurons (72). In the hippocampus, these markers are also found, but there the classical morphological classification is prioritized over immunhistochemical labels (73).

The signals mediated by VIP interneurons suggest the possibility of reinforcement learning (RL) occurring in the cerebral cortex, the mathematical algorithms of which were described as early as the 1970s (74). These algorithms are also extensively used in current artificial intelligence models, such as ChatGPT. If, in the coming years, AIs evolve to utilize not just point-like, undifferentiated neurons but also incorporate neuron types, connectomics and hierarchical structures with existing functional differences in their mathematical models, we may witness a significant new phase in their advancement.

Another important implication of these findings is that the miscalibration of RL could play a role in the development of autism spectrum disorders and schizophrenia. Therefore, unraveling the brain mechanisms of RL could bring us closer to understanding the pathophysiology of these conditions.

6. Conclusions

In this work, I have demonstrated how reinforcement signals reach the cortex. The VIP interneuron population acting as a relay, may play a crucial role in this process, and its activation could contribute to the formation of a generalized teaching signal that transiently regulates the formation and association of new memory traces with stimuli. This mode of signaling is distinct from the activation elicited by movement and does not influence participation in local sensory processing, and likely existing in multiple neuronal subtypes. The teaching signal resembles the one that was found in the dopaminergic system, with the difference that only positive prediction error signals were observed in VIP interneurons. This suggests the possibility of reinforcement learning occurring in the dorsal cortex.

7. Summary

One of the proposed functions of the cerebral cortex is the generation of complex models of the external world, which are then utilized to predict future events. These models may include information related to the impact of forthcoming events on the life prospects of living beings. Despite the critical importance of this function, the precise biological mechanisms underlying it remain obscure. In my experiments, I attempted to simulate these events with a particular emphasis on identifying the cell types and signaling pathways implicated in the cortical representation of reward and punishment. For this purpose, I employed a custom-developed 2-photon microscope with acousto-optical deflectors and special scanning modes. This advanced imaging technique allowed for the precise scanning of a sparse interneuron population, the vasoactive intestinal polypeptide (VIP) -containing interneurons. The activity of the cells was monitored with virally transfected genetically encoded calcium indicators while mice were engaged in a series of auditory discrimination tasks. In these tasks, the animals received rewards either unpredictably or in response to specific stimuli, or following a training period, they could trigger rewards through appropriate behavior. The interneurons demonstrated varied responses to the rewards and cues, and the amplitude of the response to rewards was modulated by reward expectation, distinguishable from the recruitment caused by arousal and locomotion. The reward response did not influence the cells' participation in local sensory processing. The global response pattern observed in cortical VIP interneurons indicates a specialized, cell-type-specific mechanism that enables the modulation of local neural circuitry and plasticity by integrating broader, organism-level reinforcement signals. This finding opens new avenues for understanding the complex interplay between global and local neuronal processes and their impact on learning and behavior.

8. References

1. Keller GB, Mrsic-Flogel TD. Predictive Processing: A Canonical Cortical Computation. Neuron. 2018;100(2):424-35.
2. Helmholtz HLv. Handbuch der physiologischen Optik. Leipzig: Leopold Voss; 1867.
3. Bazan AS, M. On unconscious inhibition: Instantiating repression in the brain. In: A. Fotopoulou DWPEMC, editor. From the Couch to the Lab: Trends in Psychodynamic Neuroscience: Oxford University Press; 2012. p. 307-37.
4. Sherrington CS. Observations on the sensual role of the proprioceptive nerve-supply of the extrinsic ocular muscles. Brain. 1918;41(3-4):332-3.
5. Fonyó A. Az orvosi élettan tankönyve. Budapest: Medicina Könyvkiadó Zrt.; 2011.
6. Rescola RA, Wagner AR. A theory of Pavlovian conditioning: Variations in the effectiveness of reinforcement and nonreinforcement. In: Black AH, editor. Classical conditioning: current research and theory. p. 64-96.
7. Schultz W, Dayan P, Montague PR. A neural substrate of prediction and reward. Science. 1997;275(5306):1593-9.
8. Attinger A, Wang B, Keller GB. Visuomotor Coupling Shapes the Functional Development of Mouse Visual Cortex. Cell. 2017;169(7):1291-302 e14.
9. Keller GB, Bonhoeffer T, Hubener M. Sensorimotor mismatch signals in primary visual cortex of the behaving mouse. Neuron. 2012;74(5):809-15.
10. Jordan R, Keller GB. Opposing Influence of Top-down and Bottom-up Input on Excitatory Layer 2/3 Neurons in Mouse Primary Visual Cortex. Neuron. 2020;108(6):1194-206 e5.
11. Muzzu T, Saleem AB. Feature selectivity can explain mismatch signals in mouse visual cortex. Cell Rep. 2021;37(1):109772.
12. Alm PA. The Dopamine System and Automatization of Movement Sequences: A Review With Relevance for Speech and Stuttering. Front Hum Neurosci. 2021;15:661880.
13. Lidov HG, Grzanna R, Molliver ME. The serotonin innervation of the cerebral cortex in the rat--an immunohistochemical analysis. Neuroscience. 1980;5(2):207-27.

14. Mechawar N, Cozzari C, Descarries L. Cholinergic innervation in adult rat cerebral cortex: a quantitative immunocytochemical description. J Comp Neurol. 2000;428(2):305-18.
15. Morrison JH, Molliver ME, Grzanna R. Noradrenergic innervation of cerebral cortex: widespread effects of local cortical lesions. Science. 1979;205(4403):313-6.
16. Hangya B, Ranade SP, Lorenc M, Kepecs A. Central Cholinergic Neurons Are Rapidly Recruited by Reinforcement Feedback. Cell. 2015;162(5):1155-68.
17. Robert B, Kimchi EY, Watanabe Y, Chakoma T, Jing M, Li Y, et al. A functional topography within the cholinergic basal forebrain for encoding sensory cues and behavioral reinforcement outcomes. Elife. 2021;10.
18. Laszlovszky T, Schlingloff D, Hegedus P, Freund TF, Gulyas A, Kepecs A, et al. Distinct synchronization, cortical coupling and behavioral function of two basal forebrain cholinergic neuron types. Nat Neurosci. 2020;23(8):992-1003.
19. Bouret S, Sara SJ. Reward expectation, orientation of attention and locus coeruleus-medial frontal cortex interplay during learning. Eur J Neurosci. 2004;20(3):791-802.
20. Breton-Provencher V, Drummond GT, Feng J, Li Y, Sur M. Spatiotemporal dynamics of noradrenaline during learned behaviour. Nature. 2022;606(7915):732-8.
21. Cohen JY, Amoroso MW, Uchida N. Serotonergic neurons signal reward and punishment on multiple timescales. Elife. 2015;4.
22. Hegedus P, Sviatko K, Kiraly B, Martinez-Bellver S, Hangya B. Cholinergic activity reflects reward expectations and predicts behavioral responses. iScience. 2023;26(1):105814.
23. DeFelipe J, Farinas I. The pyramidal neuron of the cerebral cortex: morphological and chemical characteristics of the synaptic inputs. Prog Neurobiol. 1992;39(6):563-607.
24. Kepecs A, Fishell G. Interneuron cell types are fit to function. Nature. 2014;505(7483):318-26.
25. Gasselin C, Hohl B, Vernet A, Crochet S, Petersen CCH. Cell-type-specific nicotinic input disinhibits mouse barrel cortex during active sensing. Neuron. 2021;109(5):778-87 e3.
26. Lee S, Kruglikov I, Huang ZJ, Fishell G, Rudy B. A disinhibitory circuit mediates motor integration in the somatosensory cortex. Nat Neurosci. 2013;16(11):1662-70.

27. Pfeffer CK, Xue M, He M, Huang ZJ, Scanziani M. Inhibition of inhibition in visual cortex: the logic of connections between molecularly distinct interneurons. Nat Neurosci. 2013;16(8):1068-76.

28. Pi HJ, Hangya B, Kvitsiani D, Sanders JI, Huang ZJ, Kepecs A. Cortical interneurons that specialize in disinhibitory control. Nature. 2013;503(7477):521-4.

29. Acsady L, Gorcs TJ, Freund TF. Different populations of vasoactive intestinal polypeptide-immunoreactive interneurons are specialized to control pyramidal cells or interneurons in the hippocampus. Neuroscience. 1996;73(2):317-34.

30. Francavilla R, Villette V, Luo X, Chamberland S, Munoz-Pino E, Camire O, et al. Connectivity and network state-dependent recruitment of long-range VIP-GABAergic neurons in the mouse hippocampus. Nat Commun. 2018;9(1):5043.

31. Hajos N, Acsady L, Freund TF. Target selectivity and neurochemical characteristics of VIP-immunoreactive interneurons in the rat dentate gyrus. Eur J Neurosci. 1996;8(7):1415-31.

32. Tyan L, Chamberland S, Magnin E, Camire O, Francavilla R, David LS, et al. Dendritic inhibition provided by interneuron-specific cells controls the firing rate and timing of the hippocampal feedback inhibitory circuitry. J Neurosci. 2014;34(13):4534-47.

33. Krabbe S, Paradiso E, d'Aquin S, Bitterman Y, Courtin J, Xu C, et al. Adaptive disinhibitory gating by VIP interneurons permits associative learning. Nat Neurosci. 2019;22(11):1834-43.

34. Williams LE, Holtmaat A. Higher-Order Thalamocortical Inputs Gate Synaptic Long-Term Potentiation via Disinhibition. Neuron. 2019;101(1):91-102 e4.

35. Ferezou I, Cauli B, Hill EL, Rossier J, Hamel E, Lambolez B. 5-HT3 receptors mediate serotonergic fast synaptic excitation of neocortical vasoactive intestinal peptide/cholecystokinin interneurons. J Neurosci. 2002;22(17):7389-97.

36. Alitto HJ, Dan Y. Cell-type-specific modulation of neocortical activity by basal forebrain input. Front Syst Neurosci. 2012;6:79.

37. Melzer S, Newmark ER, Mizuno GO, Hyun M, Philson AC, Quiroli E, et al. Bombesin-like peptide recruits disinhibitory cortical circuits and enhances fear memories. Cell. 2021;184(22):5622-34 e25.

38. Mesik L, Ma WP, Li LY, Ibrahim LA, Huang ZJ, Zhang LI, et al. Functional response properties of VIP-expressing inhibitory neurons in mouse visual and auditory cortex. Front Neural Circuits. 2015;9:22.

39. Ibrahim LA, Mesik L, Ji XY, Fang Q, Li HF, Li YT, et al. Cross-Modality Sharpening of Visual Cortical Processing through Layer-1-Mediated Inhibition and Disinhibition. Neuron. 2016;89(5):1031-45.

40. Khan AG, Poort J, Chadwick A, Blot A, Sahani M, Mrsic-Flogel TD, et al. Distinct learning-induced changes in stimulus selectivity and interactions of GABAergic interneuron classes in visual cortex. Nat Neurosci. 2018;21(6):851-9.

41. Kuchibhotla KV, Gill JV, Lindsay GW, Papadoyannis ES, Field RE, Sten TA, et al. Parallel processing by cortical inhibition enables context-dependent behavior. Nat Neurosci. 2017;20(1):62-71.

42. Sachidhanandam S, Sermet BS, Petersen CCH. Parvalbumin-Expressing GABAergic Neurons in Mouse Barrel Cortex Contribute to Gating a Goal-Directed Sensorimotor Transformation. Cell Rep. 2016;15(4):700-6.

43. Keller AJ, Dipoppa M, Roth MM, Caudill MS, Ingrosso A, Miller KD, et al. A Disinhibitory Circuit for Contextual Modulation in Primary Visual Cortex. Neuron. 2020;108(6):1181-93 e8.

44. Garcia-Junco-Clemente P, Ikrar T, Tring E, Xu X, Ringach DL, Trachtenberg JT. An inhibitory pull-push circuit in frontal cortex. Nat Neurosci. 2017;20(3):389-92.

45. Batista-Brito R, Vinck M, Ferguson KA, Chang JT, Laubender D, Lur G, et al. Developmental Dysfunction of VIP Interneurons Impairs Cortical Circuits. Neuron. 2017;95(4):884-95 e9.

46. Donato F, Rompani SB, Caroni P. Parvalbumin-expressing basket-cell network plasticity induced by experience regulates adult learning. Nature. 2013;504(7479):272-6.

47. Ferguson KA, Salameh J, Alba C, Selwyn H, Barnes C, Lohani S, et al. VIP interneurons regulate cortical size tuning and visual perception. Cell Rep. 2023;42(9):113088.

48. Fu Y, Kaneko M, Tang Y, Alvarez-Buylla A, Stryker MP. A cortical disinhibitory circuit for enhancing adult plasticity. Elife. 2015;4:e05558.

49. Kamigaki T, Dan Y. Delay activity of specific prefrontal interneuron subtypes modulates memory-guided behavior. Nat Neurosci. 2017;20(6):854-63.

50. Rahmatullah N, Schmitt LM, De Stefano L, Post S, Robledo J, Chaudhari G, et al. Hypersensitivity to Distractors in Fragile X Syndrome from Loss of Modulation of Cortical VIP Interneurons. J Neurosci. 2023;43(48):8172-88.
51. Garrett M, Manavi S, Roll K, Ollerenshaw DR, Groblewski PA, Ponvert ND, et al. Experience shapes activity dynamics and stimulus coding of VIP inhibitory cells. Elife. 2020;9.
52. Bastos G, Holmes JT, Ross JM, Rader AM, Gallimore CG, Wargo JA, et al. Top-down input modulates visual context processing through an interneuron-specific circuit. Cell Rep. 2023;42(9):113133.
53. Pinto L, Dan Y. Cell-Type-Specific Activity in Prefrontal Cortex during Goal-Directed Behavior. Neuron. 2015;87(2):437-50.
54. Turi GF, Li WK, Chavlis S, Pandi I, O'Hare J, Priestley JB, et al. Vasoactive Intestinal Polypeptide-Expressing Interneurons in the Hippocampus Support Goal-Oriented Spatial Learning. Neuron. 2019;101(6):1150-65 e8.
55. Szadai Z, Pi HJ, Chevy Q, Ocsai K, Albeanu DF, Chiovini B, et al. Cortex-wide response mode of VIP-expressing inhibitory neurons by reward and punishment. Elife. 2022;11.
56. Ramamurthy DL, Chen A, Zhou J, Park C, Huang PC, Bharghavan P, et al. VIP interneurons in sensory cortex encode sensory and action signals but not direct reward signals. Curr Biol. 2023;33(16):3398-408 e7.
57. Katona G, Szalay G, Maak P, Kaszas A, Veress M, Hillier D, et al. Fast two-photon in vivo imaging with three-dimensional random-access scanning in large tissue volumes. Nat Methods. 2012;9(2):201-8.
58. Nadella KM, Ros H, Baragli C, Griffiths VA, Konstantinou G, Koimtzis T, et al. Random-access scanning microscopy for 3D imaging in awake behaving animals. Nat Methods. 2016;13(12):1001-4.
59. Szalay G, Judak L, Katona G, Ocsai K, Juhasz G, Veress M, et al. Fast 3D Imaging of Spine, Dendritic, and Neuronal Assemblies in Behaving Animals. Neuron. 2016;92(4):723-38.
60. Judak L, Chiovini B, Juhasz G, Palfi D, Mezriczky Z, Szadai Z, et al. Sharp-wave ripple doublets induce complex dendritic spikes in parvalbumin interneurons in vivo. Nat Commun. 2022;13(1):6715.

61. Kirkcaldie MTK. Neocortex. In: Watson CR, Paxinos G, Puelles L, editors. The Mouse Nervous System. Academic Press; 2012. pp. 52–111.
62. Fu Y, Tucciarone JM, Espinosa JS, Sheng N, Darcy DP, Nicoll RA, et al. A cortical circuit for gain control by behavioral state. Cell. 2014;156(6):1139-52.
63. Reimer J, Froudarakis E, Cadwell CR, Yatsenko D, Denfield GH, Tolias AS. Pupil fluctuations track fast switching of cortical states during quiet wakefulness. Neuron. 2014;84(2):355-62.
64. Kato HK, Asinof SK, Isaacson JS. Network-Level Control of Frequency Tuning in Auditory Cortex. Neuron. 2017;95(2):412-23 e4.
65. Nelson A, Schneider DM, Takatoh J, Sakurai K, Wang F, Mooney R. A circuit for motor cortical modulation of auditory cortical activity. J Neurosci. 2013;33(36):14342-53.
66. Ren C, Peng K, Yang R, Liu W, Liu C, Komiyama T. Global and subtype-specific modulation of cortical inhibitory neurons regulated by acetylcholine during motor learning. Neuron. 2022;110(14):2334-50 e8.
67. Chen N, Sugihara H, Sur M. An acetylcholine-activated microcircuit drives temporal dynamics of cortical activity. Nat Neurosci. 2015;18(6):892-902.
68. Chubykin AA, Roach EB, Bear MF, Shuler MG. A cholinergic mechanism for reward timing within primary visual cortex. Neuron. 2013;77(4):723-35.
69. Sara SJ, Bouret S. Orienting and reorienting: the locus coeruleus mediates cognition through arousal. Neuron. 2012;76(1):130-41.
70. Hussain LS, Reddy V, Maani CV. Physiology, Noradrenergic Synapse. StatPearls. Treasure Island (FL)2024.
71. La Terra D, Bjerre AS, Rosier M, Masuda R, Ryan TJ, Palmer LM. The role of higher-order thalamus during learning and correct performance in goal-directed behavior. Elife. 2022;11.
72. He M, Tucciarone J, Lee S, Nigro MJ, Kim Y, Levine JM, et al. Strategies and Tools for Combinatorial Targeting of GABAergic Neurons in Mouse Cerebral Cortex. Neuron. 2016;92(2):555.
73. Kullander K, Topolnik L. Cortical disinhibitory circuits: cell types, connectivity and function. Trends Neurosci. 2021;44(8):643-57.

74. Tomov MS, Tsividis PA, Pouncy T, Tenenbaum JB, Gershman SJ. The neural architecture of theory-based reinforcement learning. Neuron. 2023;111(8):1331-44 e8.

9. Bibliography of the candidate's publications

Publications related to the thesis:

Szadai Z, Pi HJ, Chevy Q, Ocsai K, Albeanu DF, Chiovini B, et al. Cortex-wide response mode of VIP-expressing inhibitory neurons by reward and punishment. Elife. 2022;11.

Judak L, Chiovini B, Juhasz G, Palfi D, Mezriczky Z, Szadai Z, et al. Sharp-wave ripple doublets induce complex dendritic spikes in parvalbumin interneurons in vivo. Nat Commun. 2022;13(1):6715.

Publications not related to the thesis:

Kerekes BP, Toth K, Kaszas A, Chiovini B, Szadai Z, Szalay G, et al. Combined two-photon imaging, electrophysiological, and anatomical investigation of the human neocortex in vitro. Neurophotonics. 2014;1(1):011013.

Chiovini B, Turi GF, Katona G, Kaszas A, Palfi D, Maak P, et al. Dendritic spikes induce ripples in parvalbumin interneurons during hippocampal sharp waves. Neuron. 2014;82(4):908-24.

Szalay G, Judak L, Szadai Z, Chiovini B, Mezey D, Palfi D, et al. [Fast three-dimensional two-photon scanning methods for studying neuronal physiology on cellular and network level]. Orv Hetil. 2015;156(52):2120-6.

Szalay G, Judak L, Katona G, Ocsai K, Juhasz G, Veress M, et al. Fast 3D Imaging of Spine, Dendritic, and Neuronal Assemblies in Behaving Animals. Neuron. 2016;92(4):723-38.

Palfi D, Chiovini B, Szalay G, Kaszas A, Turi GF, Katona G, et al. High efficiency two-photon uncaging coupled by the correction of spontaneous hydrolysis. Org Biomol Chem. 2018;16(11):1958-70.

Vasanits-Zsigrai A, Majercsik O, Toth G, Csampai A, Haveland-Lukacs C, Palfi D, et al. Quantitation of various indolinyl caged glutamates as their o-phthalaldehyde derivatives by high performance liquid chromatography coupled with tandem spectroscopic detections: derivatization, stoichiometry and stability studies. J Chromatogr A. 2015;1394:81-8.

Chiovini B, Palfi D, Majoros M, Juhasz G, Szalay G, Katona G, et al. Theoretical Design, Synthesis, and In Vitro Neurobiological Applications of a Highly Efficient Two-Photon Caged GABA Validated on an Epileptic Case. ACS Omega. 2021;6(23):15029-45.

10. Acknowledgements

I personally conducted the 2-photon microscopy measurements with minor assistance from BSc and MSc students, performed 70% of the trainings and surgeries, and carried out the analysis and visualization of the results. Lidia Popara executed 30% of the animal surgeries and trainings. Hyun Pi and Quentin Chevy were responsible for the photometry recordings, data analysis and visualization, and wrote the codes necessary for controlling the behavioral protocols. The principal component analysis of my own data was conducted by Quentin Chevy, while the temporal component analysis was done by Katalin Ócsai. Gergely Szalay provided the data obtained from the visual stimulation of pyramidal cells. The microscope and motion correction software were developed by Gergely Katona and Katalin Ócsai. The research concept was formulated by Balázs Rózsa and Adam Kepecs.

I would like to thank everyone mentioned above for their contributions to my research. I would like to express my gratitude to Lídia Popara for her support that helped me complete this work. Balázs Rózsa provided continuous guidance over the years and created proper conditions for successful progress. In addition to them, I would like to thank my family, friends and colleagues for their encouragement.